International Journal of Nanomedicine

Dovepress
Taylor & Francis Group

Open Access Full Text Article

ORIGINAL RESEARCH

Scutellaria baicalensis-Derived Extracellular Vesicles Alleviate Inflammatory Bowel Disease by Inhibiting the NF-κB/NLRP3 Pathway

Rong Miao[1,2,*], Shuyi Wang[2,*], Hui Yin[2], Rui Zhu[2], Ying Yin[2], Weinian Liao[2], Shaoyan Wang[2], Jun Zhang[2], Ruihua Li[2], Junjie Xu[2]

[1]College of Pharmacy, Nanjing University of Chinese Medicine, Nanjing, 210023, People's Republic of China; [2]National Key Laboratory of Advanced Biotechnology, Academy of Military Medical Sciences, Beijing, 100071, People's Republic of China

*These authors contributed equally to this work

Correspondence: Ruihua Li; Junjie Xu, National Key Laboratory of Advanced Biotechnology, Academy of Military Medical Sciences, Beijing, 100071, People's Republic of China, Email ilovebones@163.com; xujunjie@sina.com

Background: Plant-derived extracellular vesicles (PDEV) are emerging as natural nanomedicines for various diseases. *Scutellaria baicalensis* (*S. baicalensis*) is a traditional Chinese herb long used to treat intestinal inflammatory bowel disorders (IBD), with its therapeutic effects attributed to bioactive flavonoids such as baicalin and wogonin. However, whether SEV contribute to its anti-inflammatory activity remains unexplored. The assembled multi-component nature of SEV, which carry flavonoids, lipids, proteins, and miRNAs, suggests a potential to exert therapeutic effects against IBD through mechanisms distinct from isolated compounds, with potential advantages in bioavailability and multi-target engagement.

Methods: We demonstrated that SEV exert potent antioxidant and anti-inflammatory effects in LPS-stimulated RAW264.7 macrophages and Caco-2 intestinal epithelial cells. Moreover, we assessed the therapeutic effects of SEV on dextran sulfate sodium (DSS)-induced IBD in a murine model.

Results: In inflamed RAW264.7, SEV modulated the NF-κB/NLRP3 signaling axis to exert anti-inflammatory effects. They scavenged reactive oxygen species (ROS), restored mitochondrial membrane potential, upregulated the anti-inflammatory cytokine IL-10, and suppressed the pro-inflammatory cytokines TNF-α, IL-6, and IL-1β. In Caco-2 intestinal epithelial cells, SEV also repaired intestinal barrier function by restoring expression of the tight junction proteins Zonula Occludens-1 (ZO-1), Claudin-1, and Occludin (OCLN), alongside reduced TNF-α levels. In vivo, SEV accumulated at colonic inflammatory loci to effectively alleviate IBD, as evidenced by improved body weight and increased colon length. This protective effect was mediated through inhibition of the NF-κB/NLRP3 signaling axis in colon tissues, which subsequently restored intestinal barrier integrity by increasing goblet cell numbers, upregulating OCLN proteins, and enhancing Mucin2 (MUC2) secretion, while simultaneously rebalancing inflammatory cytokines through suppression of TNF-α/IL-1β and promotion of IL-10 production.

Conclusion: SEV have the potential to protect the colon against DSS-induced colitis by inhibiting the NF-κB/NLRP3 signaling pathway, providing a promising therapeutic candidate for IBD.

Keywords: *Scutellaria baicalensis*, extracellular vesicles, inflammatory bowel disease, intestinal inflammation, oxidative stress

Introduction

Inflammatory bowel disease (IBD) refers to a group of disorders characterized by chronic inflammation of the gastrointestinal tract and is commonly associated with symptoms such as abdominal pain, weight loss, and diarrhea.[1,2] Clinically, IBD has emerged as a global burden, owing to its severe effects on patients.[3] Although several drugs have been investigated for IBD treatment in clinical trials, their efficacy and safety profiles remain suboptimal, presenting significant clinical challenges. Therefore, there is a need for alternative, mechanism-informed approaches.

https://doi.org/10.2147/IJN.S586382
Received: 19 December 2025
Accepted: 13 April 2026
Published: 27 April 2026

Graphical Abstract

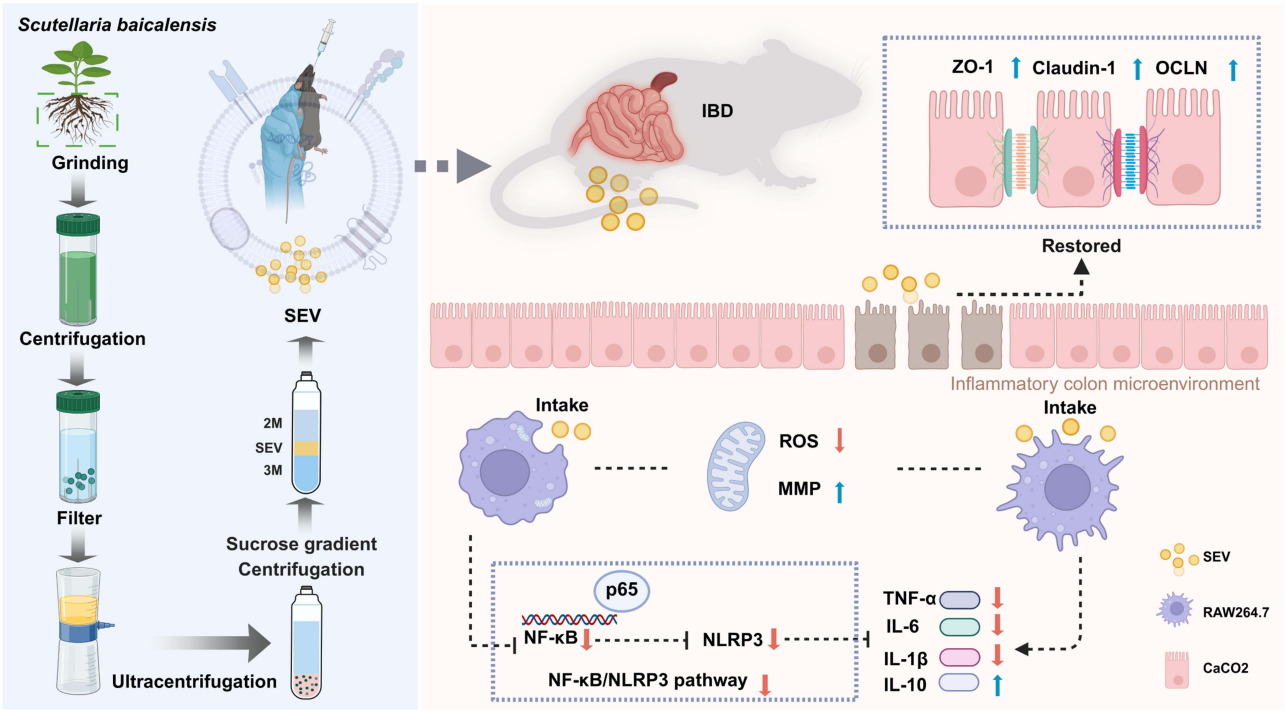

Scutellaria baicalensis (S. baicalensis) has long been described as a potent remedy for intestinal disorders, including colitis, diarrhea, and dysentery.[4] Accordingly, the active constituents of *S. baicalensis* have the potential to be developed into candidate drugs for IBD treatment, although their clinical translation may be constrained by bioavailability and targeted delivery. To address such limitations, extracellular vesicles (EV) have emerged as promising delivery systems. EV are nanoscale vesicles composed of lipids, proteins, nucleic acids, and other bioactive molecules and offer advantages such as high biocompatibility, bioavailability, multi-component synergy.[5–7] Recently, plant-derived extracellular vesicles (PDEV) derived from plants have attracted considerable research attention, not only for their intrinsic delivery capabilities but also for their enrichment of plant-sourced bioactive components.[8–11] Numerous studies have demonstrated that PDEV can be used to treat various diseases, including skin photoaging, osteoporosis, and IBD. For instance, extracellular vesicle-like nanovesicles derived from *Polygonum multiflorum*[12] exhibit photoaging-resistant properties by alleviating oxidative stress and upregulating collagen expression. Similarly, yam-derived exosome-like vesicles[13] promoted osteoblast differentiation and prevented osteoporosis in murine models. Remarkably, turmeric-derived[14] and *Coptis*-derived[11] vesicles can be easily absorbed by the intestinal tract and play critical roles in regulating intestinal epithelial homeostasis, enhancing intestinal barrier function, and modulating the gut microbiota. Collectively, these findings highlight that medicinal PDEV represent a viable therapeutic strategy for controlling colon-related disorders and promoting colonic health.

Given the therapeutic potential of both *S. baicalensis* and PDEV, we hypothesized that *Scutellaria baicalensisi*-derived extracellular vesicles (SEV) may offer a multi-component, integrated delivery system with enhanced efficacy for IBD treatment. Increasing evidence points to immune system dysfunction, aberrant reactive oxygen species (ROS) levels, and intestinal surface epithelial damage as central drivers in the pathogenesis of IBD.[15,16] Macrophages are key innate immune cells that maintain intestinal homeostasis by recognizing pathogen-associated molecular patterns via pattern recognition receptors, including Toll-like receptors and nucleotide-binding oligomerization domain-like receptors (NLRs). NLRP3, the most extensively studied member of the NLR family, is closely associated with the progression

and deterioration of IBD. Numerous recent preclinical reports have indicated that the administration of antioxidants can scavenge excessive ROS and attenuate inflammatory responses by suppressing NLRP3 inflammasome activation,[17] which triggers the secretion of IL-18 and IL-1β, thereby exacerbating the inflammatory damage of the colon.[18] The NF-κB signaling pathway has been identified as a pivotal pathway in mediating inflammatory responses. The main activators of canonical NF-κB signaling include TNF-α, IL-1β, lipopolysaccharide (LPS), and antigens, which bind to cell surface receptors and initiate NF-κB signaling via multiple bridging proteins.[19] Thus, the NF-κB/NLRP3 signaling axis has been increasingly recognized as a central pathway in IBD pathogenesis. Restoration of intestinal barrier integrity is critical in IBD management, with the expression levels of tight junction (TJ) proteins, including Zonula Occludens-1 (ZO-1), Claudin-1, and Occludin (OCLN), serving as key assessment metrics.[20] Consequently, LPS-induced inflammatory responses in the macrophage and Caco-2 cell models have become widely used experimental systems for investigating intestinal inflammatory phenotypes and their underlying molecular mechanisms.[21]

Individual components of *S. baicalensis*, such as baicalin and wogonin, have been shown to ameliorate IBD by inhibiting NF-κB signaling and NLRP3 inflammasome activation.[22–24] As an integrated delivery system, SEV may offer a more comprehensive effect compared to these single compounds. Although a recent report indicated that SEV were extracted and utilized for the treatment of colon cancer,[25] their therapeutic efficacy in IBD remains unexplored. Therefore, whether SEV exert therapeutic effects against IBD and whether these effects are mediated by the NF-κB/NLRP3 pathway remains unclear, prompting us to investigate their potential as a novel therapeutic strategy.

In summary, the present study aimed to investigate the therapeutic effect of SEV in a dextran sulfate sodium (DSS)-induced mouse model of IBD and elucidate the underlying anti-inflammatory mechanisms. First, the physicochemical properties and chemical composition of the SEV were systematically characterized. The anti-inflammatory activity of SEV was evaluated using LPS-stimulated RAW264.7 macrophages and Caco-2 intestinal epithelial cells. Finally, the regulatory effects of SEV on inflammation-associated signaling pathways were examined in the mouse model of IBD, with a specific focus on NF-κB/NLRP3 signaling and intestinal barrier integrity.

Materials and Methods

Isolation and Purification of SEV

Fresh *S. baicalensis* was purchased from a manufacturer (Weifang, Shandong Province, China) and washed thoroughly. The washed roots were weighed and homogenized in an equal volume of PBS. The mixture was stirred continuously for 10 min in a blender (VITAMIX, TNC5200, USA). The homogenate was sequentially centrifuged at 500 g for 10 min, 2000 g for 20 min, 5000 g for 20 min, and 10000 g for 60 min at 4°C (Avanti J-26 XPI; BECKMAN COULTER, USA) to remove large tissue fragments and cell debris. The supernatant was filtered through a 0.45 μm membrane and subsequently ultracentrifuged at 100000 g for 120 min at 4°C (Optima-XPN100, BECKMAN COULTER, USA). The pellet was resuspended in PBS and subjected to another round of ultracentrifugation under identical conditions. The final pellet was further purified by sucrose density gradient centrifugation (2 mol/L and 3 mol/L sucrose solutions) at 100000 g for 120 min at 4°C. The interfacial band was collected, washed with PBS, and resuspended to obtain the purified SEV. The final SEV suspension was passed through a sterile 0.22 μm filter (BS-PES25-22-S, Merck Millipore, Germany).

Characterization of SEV

The SEV protein concentration was determined using a Pierce BCA Protein Assay Kit (23225, Thermo, USA). The morphology of the SEV was observed and photographed using transmission electron microscope (TEM) (JEM-1200EX, JEOL, Japan). The particle size distribution of SEV was measured by nanoparticle tracking analysis (NTA) (Nanosight pro, Malvern, UK) and dynamic light scattering (DLS) (Zetasizer Ultra, Malvern Panalytical, UK). The particle concentration and zeta potential of SEV were measured by DLS.

The particle size distribution of SEV was measured by DLS to evaluate the particle size stability of SEV under different environments. For membrane stability assessment, SEV from the same batch were incubated with 0.02% Triton X-100 and 0.1% SDS at a 1:1 ratio (v/v) for 30 min at room temperature. For pH stability assessment, SEV were mixed with NaOH (pH > 13) and HCl (pH < 2) at a 1:1 ratio (v/v) and incubated for 30 min at room temperature. Following incubation, the samples were

immediately neutralized to pH 7.0 using the corresponding solution (0.2 mol/L NaOH for acid-treated samples; 0.2 mol/L HCl for base-treated samples). For stability assessment in simulated gastrointestinal fluids, SEV were mixed with simulated intestinal fluid (A1790, Solarbio, China) or simulated gastric fluid (A7920, Solarbio, China) and incubated at 37°C for 0, 12, and 24 h. After incubation, the samples were immediately neutralized to pH 7.0 with the corresponding solution (0.2 mol/L HCl for intestinal fluid samples; 0.2 mol/L NaOH for gastric fluid samples).

Lipidomic, Proteomic, Metabolomic and RNA Sequencing Analyses

Comprehensive multi-omics characterization of SEV, including lipidomics, proteomics, and metabolomics, was performed by Biotech Pack Scientific Co., Ltd. (Beijing, China). For lipidomic analysis, lipids were extracted from the SEV using the Folch method. The extracts were analyzed by liquid chromatography-tandem mass spectrometry (LC-MS/MS) (Dionex U3000 UHPLC, Thermo Fisher Scientific, USA), and lipid species were identified and quantified using LipidSearch software. For proteomic analysis, proteins were extracted using RIPA buffer, digested with trypsin, and analyzed using LC-MS/MS (Dionex U3000 UHPLC, Thermo Fisher Scientific, USA). Protein identification was performed using MaxQuant software and functional annotation was conducted using the Gene Ontology (GO) and Kyoto Encyclopedia of Genes and Genomes (KEGG) databases. For metabolomic analysis, lyophilized SEV were reconstituted in methanol and analyzed using LC-MS/MS (Dionex U3000 UHPLC, Thermo Fisher Scientific, USA) coupled to a high-resolution mass spectrometer (Q Exactive, Thermo Fisher Scientific, USA).

RNA sequencing was performed by Beijing Novogene Co., Ltd. (Beijing, China). Total RNA from SEV was used to construct small RNA libraries. Following 3' and 5' adaptor ligation and reverse transcription, cDNA libraries were amplified by PCR, size-selected (18–40 bp), and quantified. Qualified libraries were sequenced using the Illumina platform. Raw reads in FASTQ format were processed using Fastp software to remove adapters, poly-N reads, and low-quality sequences, yielding high-quality clean data. Quality control metrics, including Q20, Q30, and GC content, were calculated, and all downstream analyses were performed using clean reads.

Cell Culture, Cell Viability Assay and Cell Inflammation Model

RAW264.7 (ATCC TIB-71) and Caco-2 (ATCC HTB-37) human intestinal epithelial cells were obtained from the American Type Culture Collection (ATCC, USA). Both cell lines were cultured in DMEM (Gibco, 1195–065, USA) containing 10% fetal bovine serum at 37°C with 5% CO_2. To ensure consistent growth characteristics and cellular responses, RAW264.7 cells between passages 5 and 15, and Caco-2 cells between passages 20 and 30 were used for experiments. Cells were subcultured at 80–90% confluence using 0.25% trypsin-EDTA (Gibco, 25200–056, USA). All experiments were performed with cells in the logarithmic growth phase.

For the cell viability assay, the cytotoxicity of SEV towards RAW264.7 and Caco-2 cells was assessed using the MTT assay. Cells were seeded at a density of 1×10^4 cells/well in 96-well plates and incubated for 24 h with SEV at final concentrations of 12.5, 25, 50, and 100 μg/mL. Subsequently, cells were incubated with the MTT reagent (5 mg/mL) (475989, Sigma, USA) for 4 h, followed by the addition of dimethyl sulfoxide to dissolve the formazan crystals. The optical density (OD) was measured at 570 nm using a microplate reader (TECAN, Sunrise, Austria). Cell viability was calculated using the following formula: Cell viability (%) = (OD sample/mean OD control) × 100.

For the cell inflammation model, RAW264.7 cells and Caco-2 cells were seeded at a density of 2×10^5 cells/well in 6-well plates. Then the cells were first treated with lipopolysaccharide (LPS; 1 μg/mL; L2880, Sigma-Aldrich, USA) for 24 h and then co-treated with different concentrations of SEV for another 24 h. The established inflammatory model was used for downstream cellular experiments.

For the cell inhibitor experiment, RAW264.7 cells were seeded at a density of 2×10^5 cells/well in 6-well plates. After LPS (1 μg/mL; L2880, Sigma-Aldrich, USA) stimulation, these cells were treated simultaneously with SEV (100 μg/mL), MCC950 (1 μM; HY-13812, MedChemExpress, USA) and QNZ (1 nM; HY-12815, MedChemExpress, USA) for 2 h, following which LPS was introduced to induce stimulation for 24 h. The cells were then collected for protein extraction and Western blot analysis.

In vitro and in vivo SEV Uptake Assays

SEV were suspended in 1,1'-dioctadecyl-3,3,3'3' tetramethyl indocarbocyanine perchlorate (Dil) solution (V22885, Invitrogen, USA) and incubated for 30 min. Subsequently, the samples were ultracentrifuged at 100000 g for 120 min to remove unbound dye. Dil-labeled SEV were obtained for experimental use after thorough washing and resuspension in PBS.

For the in vitro experiments, Dil-labeled SEV (25 μg/mL) were incubated with RAW264.7 cells (2×10^5 cells/well) in 6-well plates for 0, 12, or 24 h. After nuclear staining with DAPI for 10 min, the cells were washed three times with PBS. Cellular uptake was visualized using a laser scanning confocal microscope (LSM900, Zeiss, Germany). For the in vivo studies, PKH26-labeled SEV (1 mg per mouse) was administered to IBD mice via intraperitoneal injection or oral gavage. After 24 hours, the fluorescence signal intensity and tissue distribution of SEV were analyzed using Living Image software (IVIS Spectrum, PerkinElmer, USA).

Oxidative Stress Assays

Fluorescent probes for dihydroethidium (DHE, 10 μM; S0063, Beyotime, China), 5,5',6,6'-Tetrachloro-1,1',3,3'-tetraethyl-imidacarbocyanine iodide (JC-1, 10 μM; C2003S, Beyotime, China), and 2',7' dichlorofluorescein diacetate (DCFH-DA, 10 μM; ID3130, Solarbio, China) were used to detect intracellular oxidative stress. All probes were incubated with the cells for 20 min at 37°C. RAW264.7 cells were washed twice with PBS and analyzed using a flow cytometer (FACSCanto II, BD Bioscience, USA), a fluorescence microplate reader (Cytation1, BioTek, USA), and fluorescence microscope (SPARK 10M, TECAN, Switzerland). Image processing was performed using FIJI-ImageJ software (version 10.8, NIH, USA). The specific fluorescently labeled antibodies used for flow cytometry were as follows: Zombie NIR Fixable Viability Kit (423105, BioLegend, USA), Anti-F4/80-PE-Cy7 (abs1850271, Absin, China), and anti-CD86-APC (abs1850141, Absin, China). Flow cytometry data were analyzed using FlowJo software (version 10.8, Tree Star Inc., USA).

Therapeutic Evaluation of SEV in a Murine DSS-Induced Colitis Model

Male C57BL/6J mice (8 weeks old, 18–22 g) were purchased from Beijing Vital River Laboratory Animal Technology Co., Ltd. (Beijing, China). A random number table was generated using SPSS software (version 26.0, IBM, USA) to assign mice into six groups. The groups were as follows: blank control, SEV-only control (1 mg SEV per mouse), DSS-induced model (2.5% DSS in drinking water), positive control (DSS+0.3 g/kg sulfasalazine) and SEV-treated groups (DSS + 0.5 mg SEV per mouse; DSS + 1 mg SEV per mouse). Colitis was induced by ad libitum administration of 2.5% DSS in drinking water for five days, after which the mice were returned to regular water. The control and SEV-only groups received normal water throughout the study. Following model induction, a 5-day treatment was initiated via daily oral gavage (0.2 mL per mouse) of PBS, sulfasalazine, or the respective SEV dose. All animals were euthanized on day 11. Serum and tissue specimens were stored at −80°C. A separate cohort of mice from the blank control and the SEV-only group (1 mg SEV per mouse) was used for toxicity assessment. Major organs were collected for histopathological examination, and blood samples were analyzed for ALT, AST, TP, CREA, and UREA levels using an automated clinical analyzer by Beijing Saveir Co., Ltd.

Assessment of Disease Activity and Histopathology in DSS-Induced Colitis Mice

Disease progression was monitored daily by recording changes in body weight and detecting fecal occult blood. On day 11, the mice were euthanized and colon lengths were measured. A blinded observer performed a macroscopic evaluation of the colons, scoring them according to criteria, including hyperemia, wall thickening, ulceration, extent of inflammation, and overall damage (see Table 1 for detailed scoring criteria). Subsequently, colonic tissues were fixed in 4% paraformaldehyde, processed, and embedded in paraffin. Tissue sections were prepared and stained with hematoxylin and eosin (H&E) by Beijing Saveir-Biotechnology Co., Ltd. (Beijing, China) for histopathological analysis, which included evaluation of inflammation severity and goblet-cell loss.

Enzyme-Linked Immunosorbent (ELISA) Assay

RAW264.7 cells (2×10^5/well) were seeded in 6-well culture plates and cultured for 24 h. LPS (1 μg/mL) was then added to the culture medium for 24 h, followed by treatment with SEV (25, 50, or 100 μg/mL) for another 24 h. The cell culture

Table 1 Macroscopic Score

Score	The Damage of Colon
0	No damage
1	Hyperemia without ulcers
2	Hyperemia and wall thickening without ulcers
3	One ulceration site without wall thickening
4	Two or more ulceration sites
5	0.5 cm extent of inflammation or major damage
6–10	1 cm extent of inflammation or severe damage

supernatants were collected. Mouse serum was obtained by centrifuging blood samples at 3000 g for 15 min at 4°C. The levels of selected cytokines (TNF-α, IL-1β, IL-6, and IL-10) in mouse serum and RAW264.7 cell supernatants were measured using commercial ELISA kits (see Table S1) according to the manufacturer's instructions.

Quantitative Real-Time PCR Assay

Total RNA was isolated from the cells using the RNA Easy Fast Tissue/Cell kit (DP451, TIANGEN, China). Complementary DNA (cDNA) was synthesized from the extracted RNA using the FastKing RT Kit (with gDNase) (KR116, TIANGEN, China). qPCR was performed using PowerUp SYBR Green Master Mix (A25742, Applied Biosystems, USA) on a QuantStudio 3 Real-Time PCR System (Applied Biosystems, Thermo Fisher Scientific, USA). The primer sequences used for gene amplification are listed in Table S2.

Western Blot WB

Proteins were extracted from SEV, cells or tissues using RIPA lysis buffer (P0013B, Beyotime, China), and the protein concentration was measured using a BCA Protein Assay kit (23225, Thermo Scientific, USA). Samples were mixed by the addition of 5 × SDS-PAGE loading buffer (P0015L, Beyotime, China) and heated at 100°C for 10 min. Proteins were separated by 4–12% Bis-Tris precast gels (M00652/M00654, Genscript, China) by sodium dodecyl sulfate-polyacrylamide gelelectrophoresis (SDS-PAGE), transferred to nitrocellulose membranes, and blocked with 5% skim milk in PBS containing 0.1% (v/v) Tween20 (0.1% PBST). Membrane was then washed with 0.1% PBST, incubated with primary antibodies overnight at 4°C, followed by horseradish peroxidase (HRP) conjugated secondary antibody for 45 min at room temperature. Protein bands were visualized using an ECL chemiluminescence Kit (WBKLS0500, Millipore, USA) and imaged with a chemiluminescence imaging system. Band intensity was quantified using FIJI-ImageJ software (version 10.8, NIH, USA). The antibodies used are listed in Table S3.

Statistical Analysis

All data are presented as the mean ± standard deviation (SD) from at least three independent experiments. Statistical analyses were performed using GraphPad Prism software (version 10.0, Graphpad Software, USA). Comparison between multiple groups were conducted using one-way or two-way ANOVA followed by Tukey's multiple comparisons test. A p-value of less than 0.05 was considered statistically significant.

Results

SEV are Successfully Isolated and Characterized

SEV were isolated and purified from the root juice of *S. baicalensis* using a two-step centrifugation protocol: differential centrifugation followed by sucrose density gradient ultracentrifugation (Figure 1A). Specifically, the root juice was first subjected to sequential low-speed centrifugation to remove cellular debris and large aggregates and then ultracentrifuged to

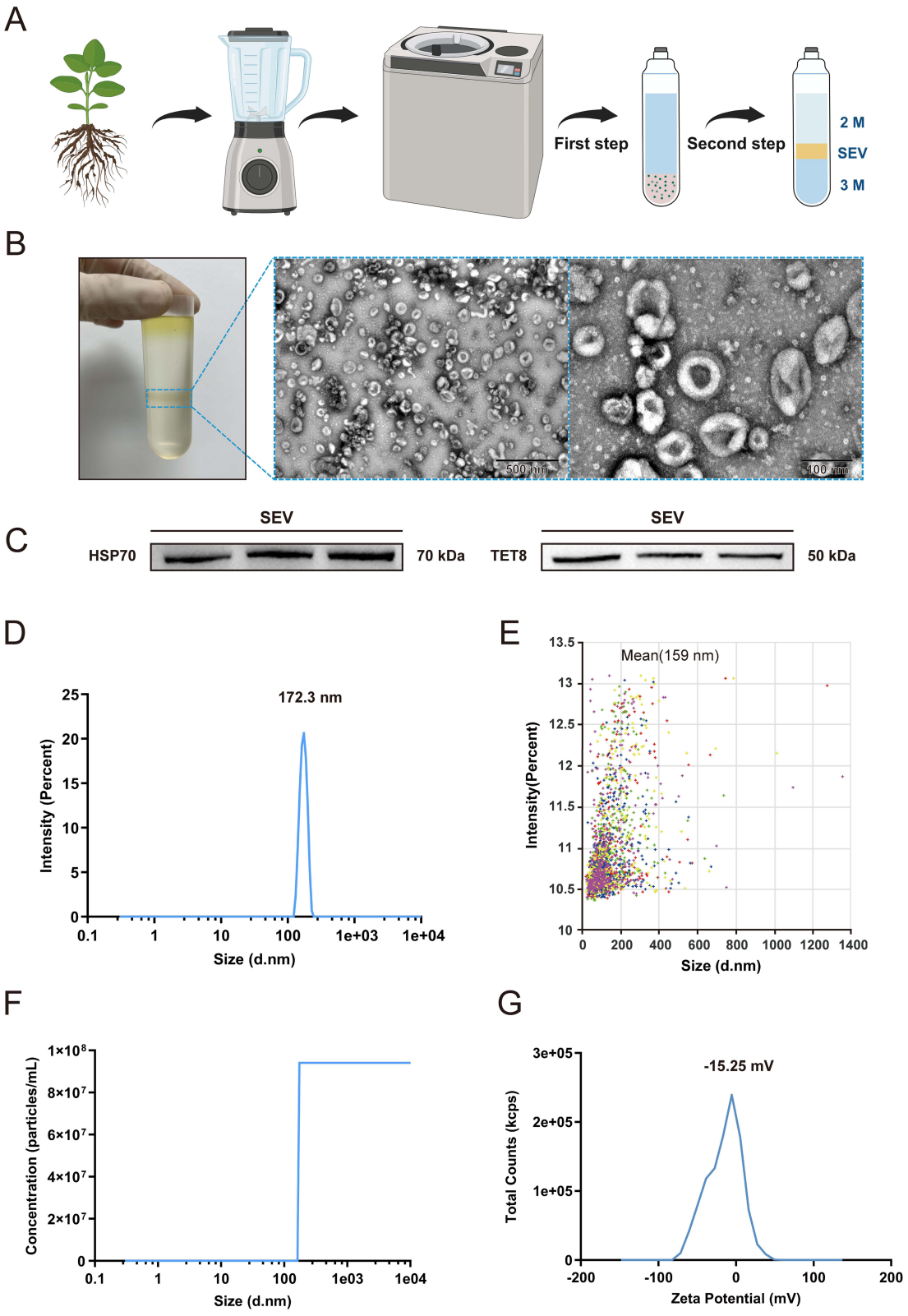

Figure 1 Preparation and identification of SEV. (**A**) SEV were obtained by cell disruption, ultracentrifugation, and 2 mol/L-3 mol/L sucrose density gradient ultracentrifugation. (**B**) The fraction indicated by the blue frame was collected for transmission electron microscopy (TEM) imaging, with scale bars of 500 nm and 100 nm, respectively. (**C**) Detection of vesicle markers TET8 and HSP70 by Western blot. (**D**) Size distribution of SEV detected by Dynamic Light Scattering (DLS). (**E**) Size distribution of SEV detected by nanoparticle tracking analysis (NTA). (**F**) Particle concentration of SEV measured by DLS. (**G**) Zeta potential of SEV measured by DLS.

https://doi.org/10.2147/IJN.S586382

pellet crude SEV, which were further purified via a 2–3 mol/L sucrose density gradient to eliminate protein contaminants. Transmission electron microscopy (TEM) analysis revealed that the SEV exhibited a spherical or cup-shaped morphology with distinct a lipid bilayer (Figure 1B), and the presence of the classical vesicle markers HSP70 and TET8 was confirmed by Western blotting (Figure 1C). The particle size ranged from 150 to 200 nm, with average diameters of 172.3 nm and 159 nm measured by dynamic light scattering (DLS) and nanoparticle tracking analysis (NTA), respectively (Figure 1D and E). The particle concentration of SEV, measured in a 100-fold diluted sample, was 9.41×10^7 particles/mL, corresponding to an estimated original concentration of approximately 1×10^{10} particles/mL (Figure 1F). The Zeta potential averaged −15.25 mV (Figure 1G), indicating a negative surface charge that promotes colloidal stability.

Changes in vesicle particle size under different conditions serve as an important method for assessing their stability. First, after treatment with 0.02% Triton X-100 and 0.1% SDS, the particle size distribution of SEV shifted from unimodal to multimodal, indicating disruption of the vesicle structure (Figure S3A). Under acidic and alkaline conditions, SEV maintained a unimodal particle size distribution with a slight shift, along with increased particle size and volume expansion (more pronounced under acidic conditions). Nevertheless, SEV retained a membranous vesicle structure in both acidic and alkaline environments, with no significant rupture (Figure S3B). To predict the in vivo behavior of SEV, their stability was evaluated under key physiological conditions by simulating gastric and intestinal fluids in vitro. The results showed that the particle size distribution of SEV remained stable during incubation in PBS and simulated intestinal fluid at 37°C for up to 24 h (Figure S3C-E). These findings indicate that SEV exhibit a certain degree of resistance to acidic, alkaline, and gastrointestinal fluids.

SEV are Comprehensively Profiled at the Molecular Level

To systematically characterize the molecular composition of SEV derived from *S. baicalensis*, we performed a multi-omics analysis. We first investigated the lipid constituents of purified SEV by liquid chromatography-tandem mass spectrometry (LC-MS/MS). Our lipidomic profiling identified 223 distinct lipid species categorized into 7 subclasses (Figure 2A), with notable enrichment in glycerophospholipids (GPs, 29.60%) and fatty acids (FAs, 21.08%). These lipid subgroups are essential intermediates in lipid metabolism and play critical roles in lipid catabolism.[26,27] In addition to their structural contributions to membrane integrity, GPs have been implicated in cellular metabolism, signal transduction, and cell type-specific processes in mammals.[28] Notably, dietary plant-derived FAs have been shown to promote short-chain fatty acids (SCFAs) in the gut, which in turn can suppress NF-κB-STAT pathways,[29] thereby alleviating intestinal disorders.

To characterize the small RNA (sRNA) profile of SEV, we performed high-throughput sequencing of SEV. Our analysis revealed a diverse sRNA population, with transfer RNA (tRNA) accounting for the majority (68.33% of the total; Figure 2B). Among the detected sRNAs, microRNAs (miRNAs), which are critical for EV biological activity, were also present. Analysis of miRNA fragment lengths indicated a predominant size of 26 nt (Figure 2C), implying the potential presence of specific miRNA isoforms that may contribute to EV-mediated regulatory functions.

The proteomic analysis of SEV identified and quantified 59 proteins, with those ranging from 50 to 60 kDa representing the most abundant fraction (Figure 2D). After performing a gene ontology (GO) analysis (Figure 2G), we confirmed that SEV is linked to various biological phenomena, most notably including diverse metabolic and cellular processes, and possess molecular functions related to oxidative stress. Kyoto Encyclopedia of Genes and Genomes (KEGG) analysis (Figure 2H) identified glyoxylate and dicarboxylate metabolism as the most significantly enriched pathway, closely associated with oxidative stress responses.

Finally, to determine whether SEV encapsulated the characteristic bioactive metabolites of *S. baicalensis*, we performed metabolomic profiling using LC-MS/MS. A total of 125 metabolites were identified, with flavonoids representing the most abundant class (30.40% of all the detected metabolites; Figure 2E). KEGG functional enrichment analysis revealed that these metabolites were significantly associated with a broad range of biological metabolic processes (Figure 2F). Through cross-referencing with the Traditional Chinese Medicine Systems Pharmacology (TCMSP) database, we identified five known bioactive constituents in SEV. Among these shared metabolites, wogonin was the most abundant, followed by β-sitosterol, acacetin, dihydrooroxylin A, and baicalin, all of which exert reported anti-inflammatory and antioxidant effects.

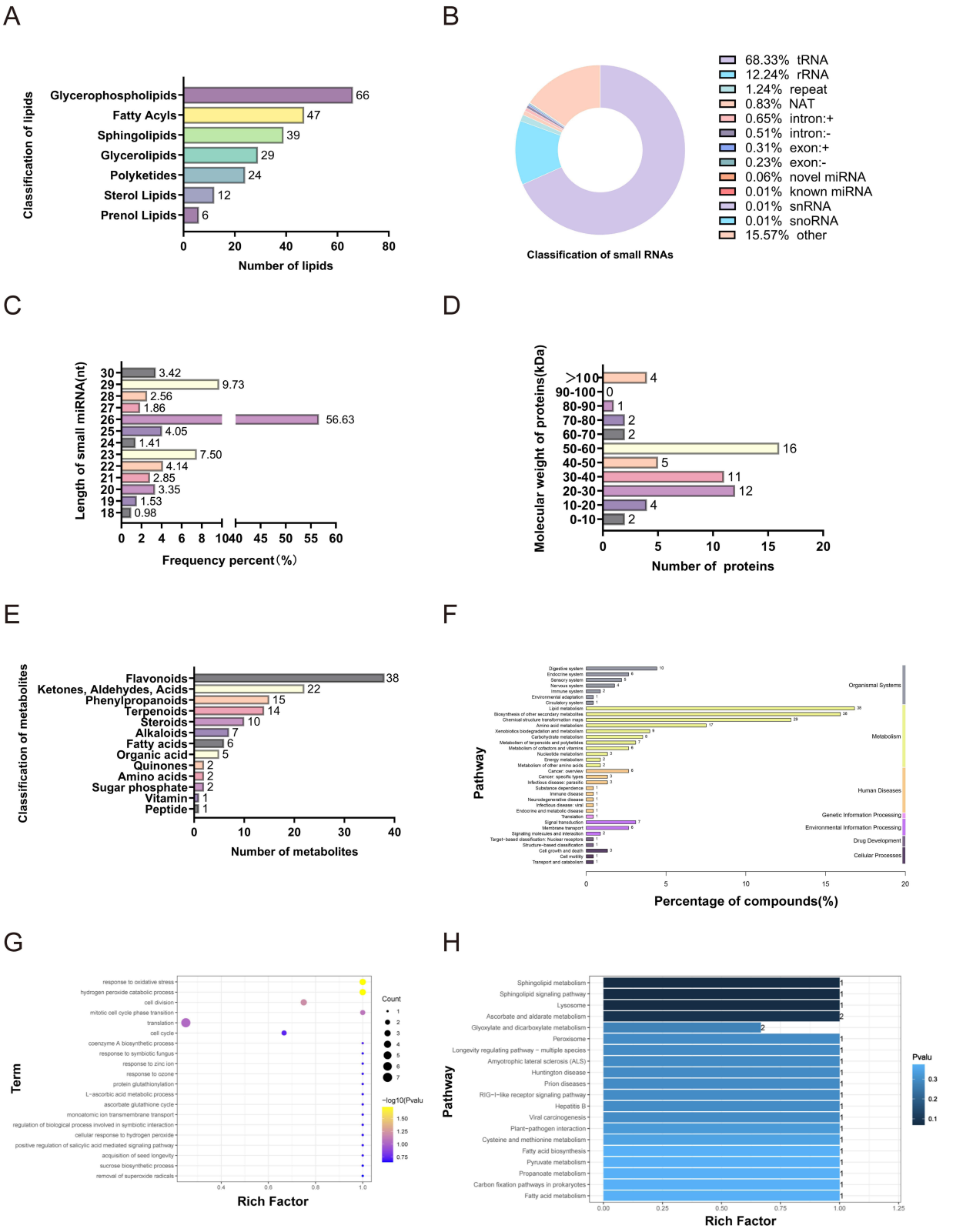

Figure 2 Characterization of SEV. (**A**) Classification of lipids in SEV. (**B**) Small RNA composition of SEV. (**C**) Length distribution of miRNA fragments in SEV. (**D**) Molecular weight of proteins in SEV. (**E**) Classification of Metabolites in SEV. (**F**) Kyoto Encyclopedia of Genes and Genomes (KEGG) pathway enrichment analysis of significantly upregulated metabolites in SEV. The Y-axis represents KEGG pathways and the X-axis represents rich factor. The color of the column represents enrichment significance and the length of the column represents number of upregulated metabolites. (**G**) Gene ontology (GO) analysis of significantly upregulated proteins in SEV. The Y-axis represents GO terms and the X-axis represents rich factor. The color of the bubble represents enrichment significance and the size of the bubble represents number of upregulated proteins. (**H**) KEGG pathway enrichment analysis of significantly upregulated proteins in SEV. The Y-axis represents KEGG pathways and the X-axis represents rich factor. The color of the column represents enrichment significance and the length of the column represents number of upregulated proteins.

https://doi.org/10.2147/IJN.S586382

SEV are Efficiently Taken up by Macrophages and Accumulate in the Colon Upon Oral Administration

To evaluate the therapeutic efficacy of SEV for inflammatory bowel disease, we first investigated their biodistribution using a DSS-induced IBD mouse model. In vivo imaging after 24 h of administration revealed that PKH26-labeled SEV were present in multiple organs, including the liver, stomach, cecum, and intestine-following both intraperitoneal (*i.p.)* and oral gavage (*ig.)* routes (Figure 3A). Notably, strong fluorescence was observed specifically in the colon of orally administered mice, whereas the intraperitoneal group showed a negligible signal, indicating that oral delivery enables efficient colonic accumulation of SEV, which is a key prerequisite for local anti-inflammatory action. Macrophages are central drivers of IBD pathogenesis, contributing to the initiation, perpetuation, and resolution of intestinal inflammation through their dual roles in immune surveillance and maintenance of barrier integrity. Next, we sought to determine whether SEV could be internalized by immune cells relevant to IBD pathogenesis. Using RAW264.7 macrophages, we

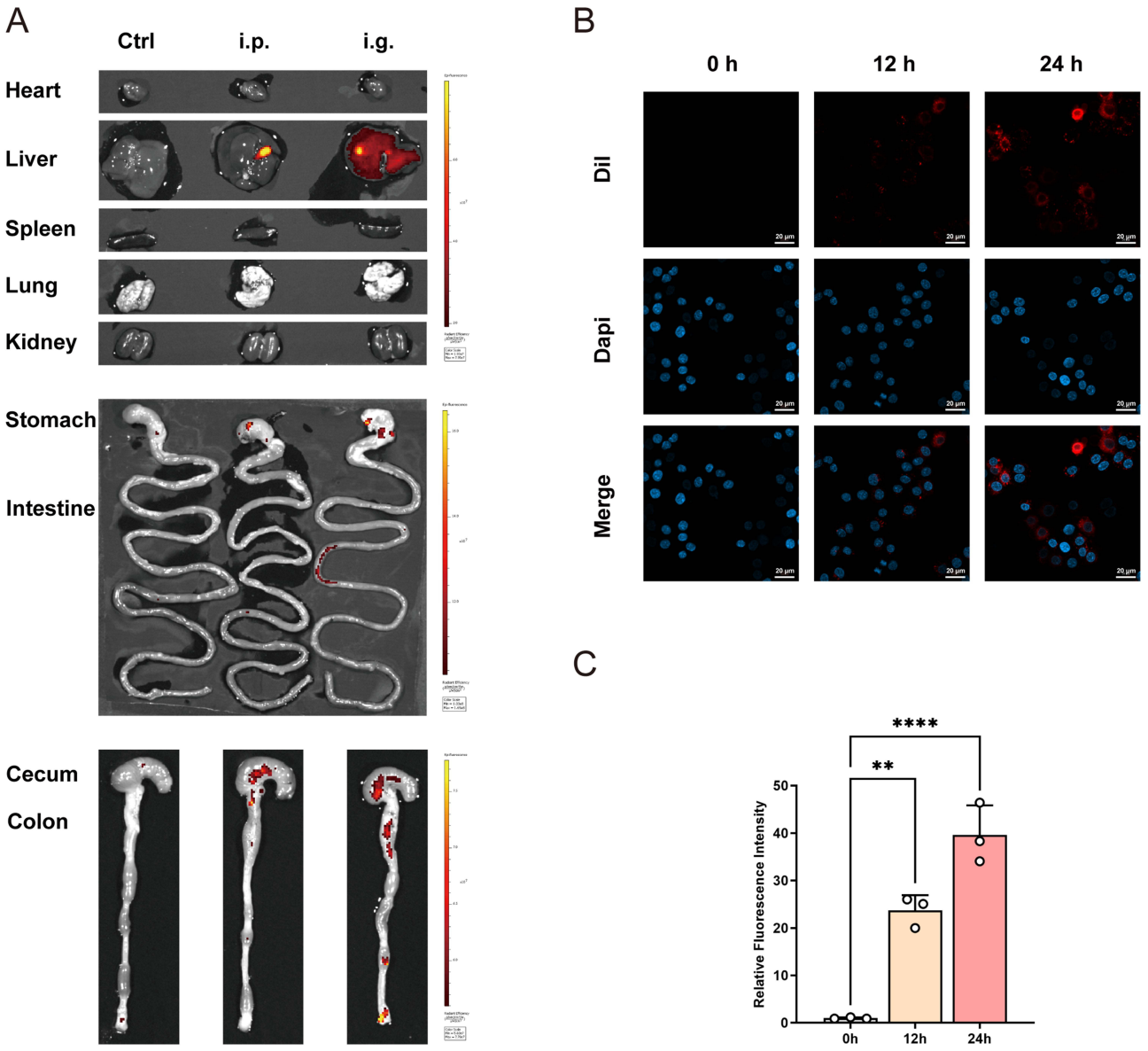

Figure 3 Biodistribution and cellular uptake and of SEV. (**A**) Tracking of PKH26-labeled SEV in IBD mice tissues at 24 h by IVIS Spectrum imaging (PKH26: excitation = 551 nm; emission = 567 nm). (**B**) Confocal images of RAW264.7 macrophages treated with DiI-labeled SEV (red) at different time points (0 h, 12 h, and 24 h) (DiI: excitation = 549 nm; emission = 565 nm; Scale bar: 20 μm). Blue represents the nucleus. (**C**) Quantification of SEV uptake over time. Data are expressed as mean ± SD (n = 3). Statistical significance was determined by one-way ANOVA followed by Tukey's post hoc test; $^{**}p < 0.01$ and $^{****}p < 0.0001$.

performed in vitro uptake assays. Confocal microscopy confirmed the internalization of DiI-labeled SEV into these immune cells (Figure 3B). Quantitative analysis further demonstrated that SEV uptake increased over time, with higher levels observed at 24 h ($p < 0.0001$; Figure 3C) compared to 12 h ($p < 0.01$; Figure 3C). Taken together, these findings establish that orally administered SEV preferentially home to the colon in vivo and are efficiently taken up by macrophages in vitro, underscoring their potential as a novel therapeutic strategy for IBD.

SEV Protect Against LPS-Induced Mitochondrial Dysfunction by Attenuating Oxidative Stress

Building on the observed cellular uptake of SEV by macrophages, we hypothesized that SEV might exert protective effects by modulating oxidative stress and mitochondrial function. To test this, we first evaluated intracellular reactive oxygen species (ROS) levels in LPS-stimulated RAW264.7 cells using dihydroethidium (DHE) staining. Flow cytometric analysis demonstrated that pretreatment with SEV significantly attenuated the LPS-induced elevation of ROS in a dose-dependent manner ($p < 0.01$, $p < 0.0001$; Figure 4A and B). This antioxidant effect was further confirmed by independent fluorescence microplate assays ($p < 0.01$ to $p < 0.0001$; Figure 4C), collectively establishing the capacity of SEV to mitigate oxidative stress in activated macrophages. We next investigated whether the SEV-mediated reduction in ROS could preserve mitochondrial membrane potential (MMP), a critical indicator of mitochondrial health. Using the JC-1 probe, we observed that LPS stimulation caused a pronounced loss of MMP, as indicated by a shift from red JC-1 aggregates (characteristic of healthy mitochondria) to green monomers (Figure 4E). Importantly, SEV treatment reversed this effect in a dose-dependent manner, restoring the red/green fluorescence ratio ($p < 0.01$, $p < 0.0001$; Figure 4D). These findings indicate that SEV not only reduce excess ROS but also prevent LPS-induced mitochondrial depolarization, thereby maintaining mitochondrial functional integrity.

SEV Attenuate LPS-Induced Inflammatory Responses by Suppressing the NF-κB/NLRP3 Signaling Axis and Modulating Macrophage Polarization

To systematically investigate the anti-inflammatory mechanism of SEV, we focused on the NF-κB/NLRP3 signaling axis, a key pathway that regulates innate immune responses. Western blot analysis revealed that treatment with SEV significantly reduced the protein expression of NLRP3 ($p < 0.01$; Figure 5A and B) and phosphorylated NF-κB p65 protein levels in LPS-stimulated RAW264.7 macrophages ($p < 0.05$; Figure 5A and C). Future results clearly demonstrated the suppressive effects of SEV, as well as inhibitors targeting NLRP3 inflammasome (MCC950) and NF-kB pathway (QNZ), on the expressions of key proteins involved in the signaling cascade, composing of NLRP3 and phosphorylated NF-κB p65 ($p < 0.05$ to $p < 0.0001$; Figure S4A–C). Having established the suppression of this key signaling pathway, we next assessed whether SEV modulates the expression of inflammatory cytokines downstream of NF-κB and NLRP3. Quantitative analysis revealed that SEV dose-dependently inhibited LPS-induced upregulation of the pro-inflammatory cytokines TNF-α and IL-6 at both the mRNA and protein levels ($p < 0.01$, $p < 0.0001$; Figure 5D, E, H and I), while concurrently enhancing the expression of the anti-inflammatory cytokine IL-10 ($p < 0.01$ to $p < 0.0001$; Figure 5F and J). However, there was no difference in TGF-β (Figure 5G). Furthermore, SEV significantly attenuated LPS-induced IL-1β expression in a dose-dependent manner ($p < 0.01$, $p < 0.0001$; Figure 5K), which was consistent with the observed inhibition of NLRP3 inflammasome activation.

Macrophages exist on a functional continuum and are classically polarized into pro-inflammatory M1 and anti-inflammatory M2 phenotypes. Given the critical role of macrophage polarization in inflammatory responses, we further investigated whether SEV influence M1/M2 phenotypic balance. Flow cytometric analysis showed that treatment with SEV significantly reduced the proportion of LPS-induced M1 macrophages in a dose-dependent manner ($p < 0.0001$; Figure 5L and M). This shift was corroborated at the transcriptional level ($p < 0.001$ to $p < 0.0001$; Figure 5N), with the lowest SEV dose (25 μg/mL) showing no significant effect, further confirming the dose-dependent effect of SEV on macrophage polarization. Our findings revealed that SEV alleviated LPS-induced inflammatory responses by concurrently inhibiting the NF-κB/NLRP3 signaling axis, restoring cytokine balance, and attenuating M1 macrophage polarization. Collectively, as an integrated platform, SEV exert multifaceted therapeutic effects through combined antioxidant, immunomodulatory, and anti-inflammatory actions.

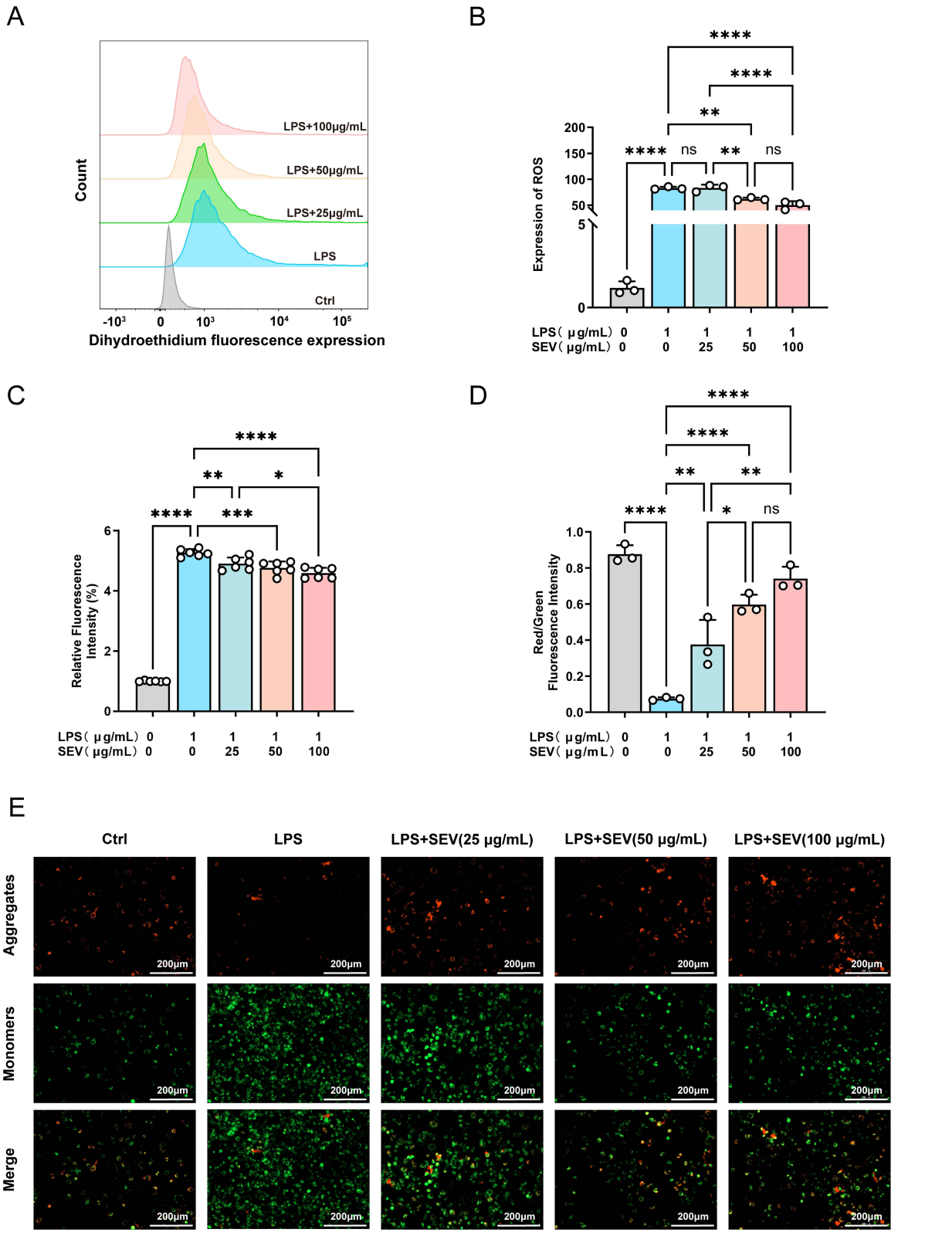

Figure 4 SEV attenuate LPS-induced oxidative stress and mitochondrial dysfunction in RAW264.7 macrophages. (**A**) Flow cytometric analysis of DHE fluorescence intensity. Cells were treated as indicated, stained with DHE, and analyzed by flow cytometry. DHE fluorescence reflects intracellular ROS levels. (**B**) Quantification diagram of DHE by FlowJo 10.8 software (n = 3). (**C**) The levels of superoxide anion (O_2^-) were quantified by a fluorescence microplate reader (n = 6). (**D**) JC-1 fluorescence was quantified by calculating the red/green ratio with ZEN software (n = 3). (**E**) Changes in intracellular MMP were observed by Fluorescence Microscope. Red fluorescence indicates JC-1 aggregates (normal MMP), while green fluorescence indicates JC-1 monomers (depolarized mitochondria). Scale bar: 200 μm. Data are expressed as mean ± SD. Statistical significance was determined by one-way ANOVA followed by Tukey's post hoc test; ns $p > 0.05$, *$p < 0.05$, **$p < 0.01$, ***$p < 0.001$, ****$p < 0.0001$.

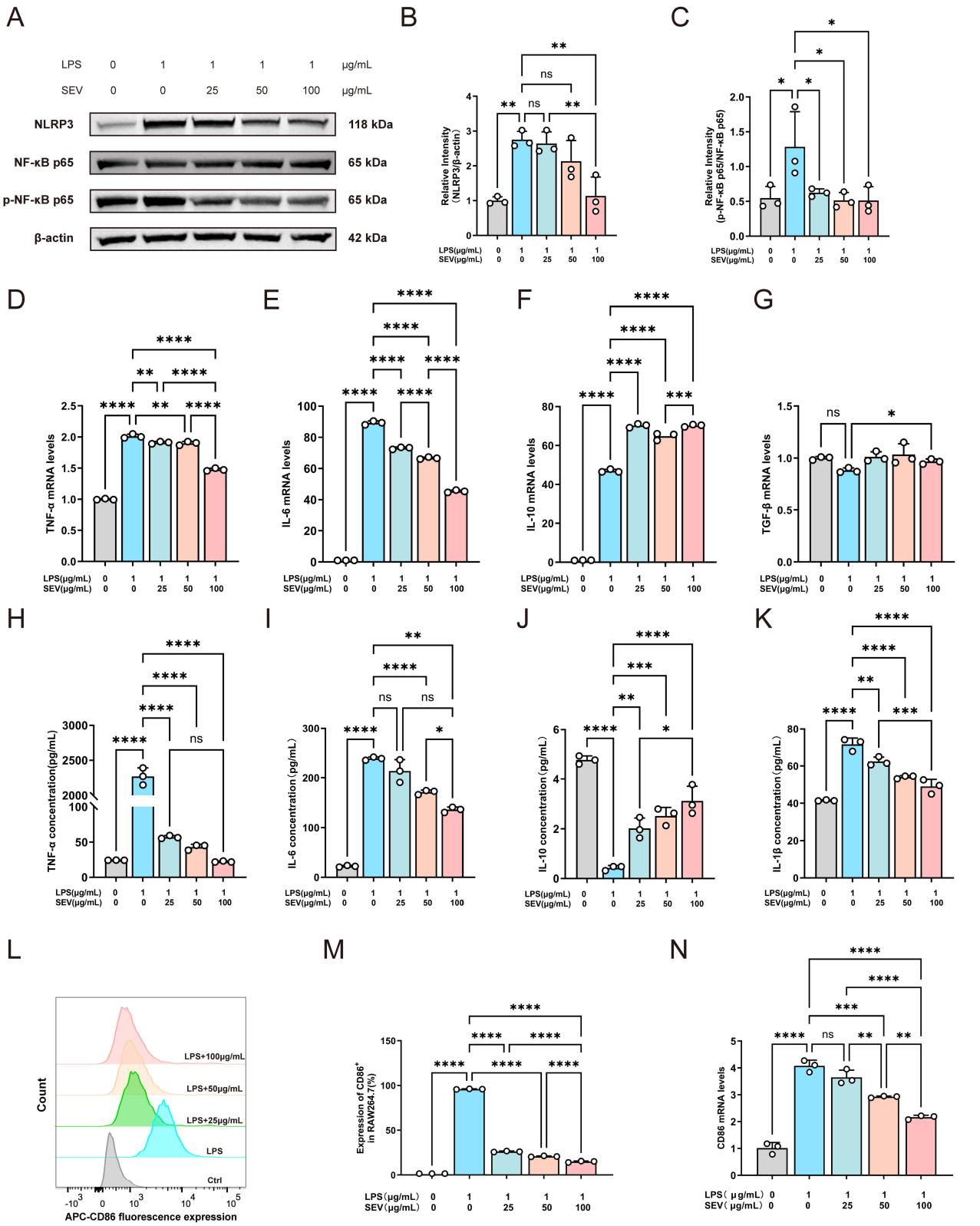

Figure 5 SEV attenuate inflammatory responses in LPS-stimulated RAW264.7 macrophages via the NF-κB/NLRP3 pathway. (**A**) Western blot images showing expression of NLRP3, total NF-κB and phosphorylated NF-κB (p-NF-κB p65) in LPS-stimulated RAW264.7 macrophages treated with or without different doses of SEV. Representative images from at least 3 independent biological replicates are shown. (**B**) Relative expression of NLRP3. (**C**) Relative expression of p-NF-κB p65. (**D**–**G**) mRNA levels of inflammatory cytokines measured by qPCR. (**D**) TNF-α, (**E**) IL-6, (**F**) IL-10, (**G**) TGF-β (n = 3). (**H**–**K**) Cytokine levels in cell culture supernatants measured by ELISA: (**H**) TNF-α, (**I**) IL-6, (**J**) IL-10, (**K**) TGF-β (n = 3). (**L**) Flow cytometric analysis of CD86 expression in macrophages to evaluate the effect of SEV on M1 polarization. (**M**) Quantification of M1 macrophages analyzed using FlowJo 10.8 software (n = 3). (**N**) mRNA expression of the M1 marker CD86 measured by RT-PCR (n = 3). Data are expressed as mean ± SD. Statistical significance was determined by one-way ANOVA followed by Tukey's post hoc test; ns $p > 0.05$, *$p < 0.05$, **$p < 0.01$, ***$p < 0.001$, ****$p < 0.0001$.

https://doi.org/10.2147/IJN.S586382

SEV Enhance Intestinal Barrier Integrity by Upregulating Tight Junction Proteins in LPS-Stimulated Caco-2 Cells

Based on our findings that SEV suppressed inflammatory responses in immune cells, we hypothesized that SEV might also protect intestinal barrier function, which is a critical component in IBD pathogenesis. To test this hypothesis, we investigated whether SEV attenuated cytokine-induced barrier damage by modulating tight junction protein expression in human intestinal epithelial Caco-2 cells. First, we examined the effect of SEV on the expression of tight junction components at the transcriptional level. qPCR analysis revealed that SEV treatment significantly and dose-dependently upregulated mRNA expression of ZO-1 ($p < 0.01$, $p < 0.0001$; Figure 6A), claudin-1 ($p < 0.0001$; Figure 6B), and OCLN ($p < 0.0001$; Figure 6C) in LPS-stimulated Caco-2 cells. Western blot analysis further confirmed that SEV intervention

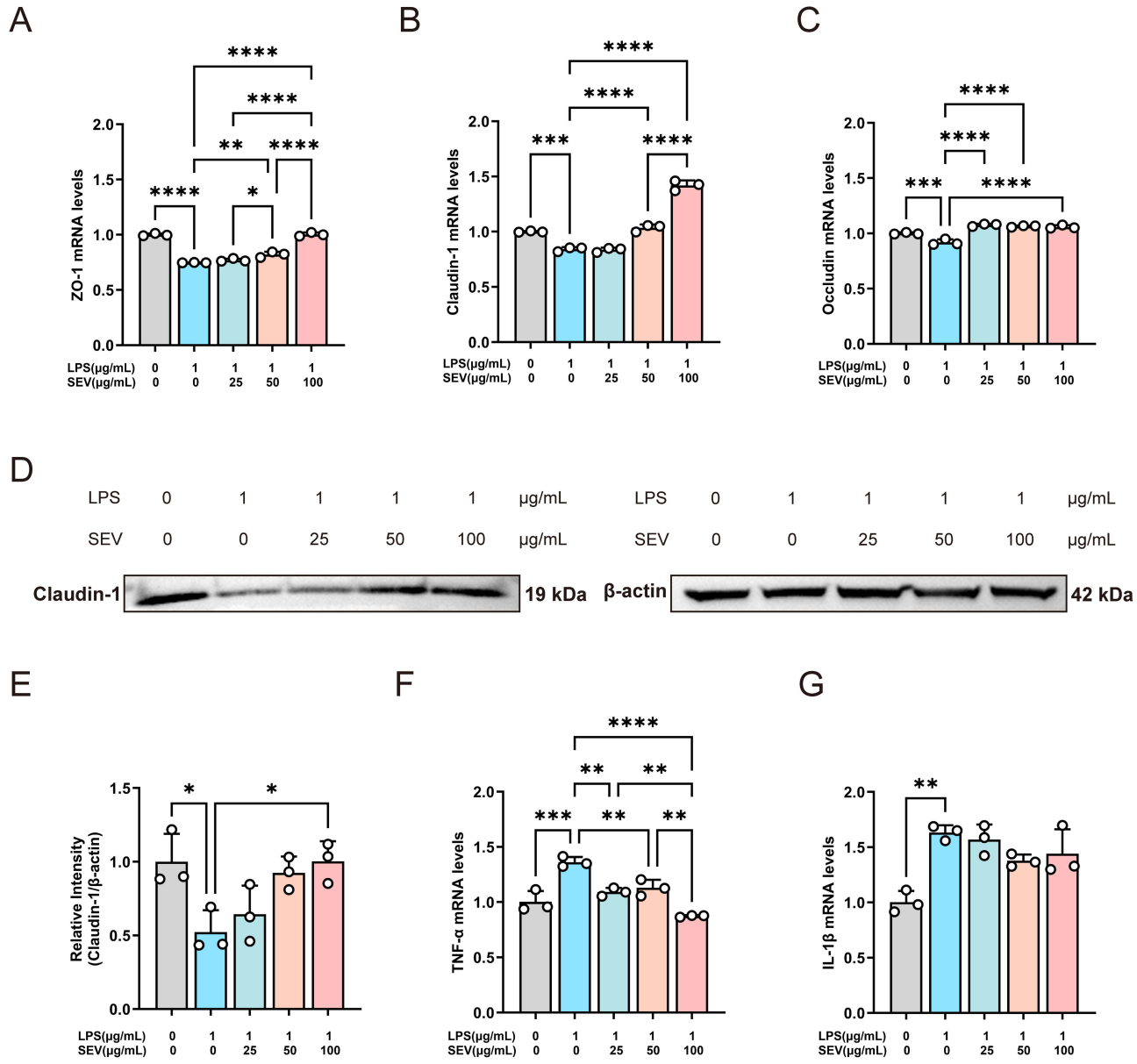

Figure 6 SEV enhance intestinal barrier integrity in LPS-stimulated Caco-2 cells. (**A**–**C**) mRNA levels in LPS-stimulated Caco-2 cells treated with or without SEV measured by qPCR. (**A**) ZO-1, (**B**) Claudin-1, (**C**) Occludin (OCLN) (n = 3). (**D**) Western blot images showing Claudin-1 expression. Representative images from at least 3 independent biological replicates are shown. β-Actin served as a loading control. (**E**) Quantification of Claudin-1 expression level (n = 3). (**F** and **G**) Cytokine levels in cell-culture supernatants measured by ELISA. (**F**) TNF-α, (**G**) IL-1β (n = 3). Data are expressed as mean ± SD. Statistical significance was determined by one-way ANOVA followed by Tukey's post hoc test; *$p < 0.05$, **$p < 0.01$, ***$p < 0.001$, ****$p < 0.0001$.

reversed the LPS-induced downregulation of tight junction protein Claudin-1 ($p < 0.05$; Figure 6D and E), demonstrating a consistent protective effect at both transcriptional and translational levels. To determine whether SEV also modulate inflammatory responses in epithelial cells, we quantified the secretion of pro-inflammatory cytokines. Notably, SEV treatment significantly reduced TNF-α release ($p < 0.01$, $p < 0.0001$; Figure 6F) but did not significantly affect IL-1β levels compared with the LPS group (Figure 6G), suggesting a selective anti-inflammatory mechanism in intestinal epithelial cells that differs from the broader cytokine suppression observed in macrophages. Collectively, these findings demonstrate that SEV not only alleviate specific inflammatory responses in intestinal epithelial cells but also enhance barrier integrity by restoring the expression of critical tight junction proteins, thereby targeting both immune and structural components of intestinal homeostasis.

SEV Ameliorate DSS-Induced Inflammatory Bowel Disease in Mice

Based on our in vitro findings demonstrating the anti-inflammatory and barrier-protective properties of SEV, we next evaluated their therapeutic potential in vivo using a DSS-induced murine model of IBD, with clinical symptoms similar to those of human colitis (Figure 7A). Oral administration of SEV (1 mg per mouse) significantly attenuated the characteristic body-weight loss associated with DSS-induced colitis ($p < 0.0001$; Figure 7B). Consistent with this improvement, high-dose SEV treatment markedly improved macroscopic scores ($p < 0.001$; Figure 7C), which were composed of indicators such as bleeding, ulcers, and inflammation, as detailed in Table S1. DSS treatment resulted in substantial colon shortening in IBD mice, and SEV treatment restored colon length to approximately 90% of the normal level ($p < 0.01$; Figure 7D and E). Histopathological examination of colon tissue provided further evidence of SEV-mediated protection. H&E staining revealed that DSS-treated mice exhibited severe colonic damage, characterized by extensive inflammatory cell infiltration, loss of goblet cells, and disruption of crypt architecture. Notably, these pathological changes were substantially ameliorated by SEV treatment, as reflected by the significantly normalized goblet cell numbers in the intestinal glands ($p < 0.001$; Figure 7F and Figure S1). In summary, these results demonstrate that SEV effectively mitigate the progression of DSS-induced colitis, preserve colon morphology, and reduce disease severity, thereby supporting its potential as a promising therapeutic candidate for inflammatory bowel disease.

SEV Attenuate DSS-Induced Inflammatory Bowel Disease in Mice by Inhibiting NF-κB/NLRP3 Signaling Axis

To validate the anti-inflammatory mechanism of SEV observed in vitro, we investigated whether their protective effects in vivo were associated with modulation of the NF-κB/NLRP3 signaling axis. Western blot analysis of colon tissues demonstrated that DSS administration significantly induced the overexpression of NLRP3 and phosphorylated NF-κB p65 compared with that in the control group ($p < 0.05$; Figure 8A–C). Importantly, SEV treatment (1 mg per mouse) markedly reversed these alterations, substantially reducing NLRP3 and phosphorylated NF-κB p65 protein levels ($p < 0.01$; Figure 8A–C).

Next, we assessed whether the suppression of inflammatory signaling translated into improved intestinal barrier integrity and systemic anti-inflammatory effects. Western blot analysis revealed that DSS administration severely reduced the expression of the tight junction protein OCLN in colon tissues, an impairment that was significantly rescued by SEV treatment, with efficacy matching that of the SASP ($p > 0.05$; Figure 8A and D). Immunofluorescence results revealed that the MUC2 protein, which is essential for intestinal lubrication and barrier integrity, was significantly upregulated by SEV treatment ($p < 0.05$; Figure 8E and Figure S2). Furthermore, serum cytokine analysis showed that SEV not only suppressed the DSS-induced elevation of pro-inflammatory cytokines (TNF-α and IL-1β; $p < 0.0001$; Figure 8F and G) but also significantly increased the production of the anti-inflammatory cytokine IL-10 ($p < 0.001$, $p < 0.0001$; Figure 8H), outperforming the SASP group ($p < 0.01$, Figure 8H).

In conclusion, these in vivo results demonstrate that the therapeutic efficacy of SEV in experimental colitis is mechanistically linked to the suppression of the NF-κB/NLRP3 signaling pathway, restoration of intestinal barrier integrity, and rebalancing of systemic inflammatory and anti-inflammatory cytokine responses. These dual effects may be attributed to the multicomponent nature of SEV.

https://doi.org/10.2147/IJN.S586382

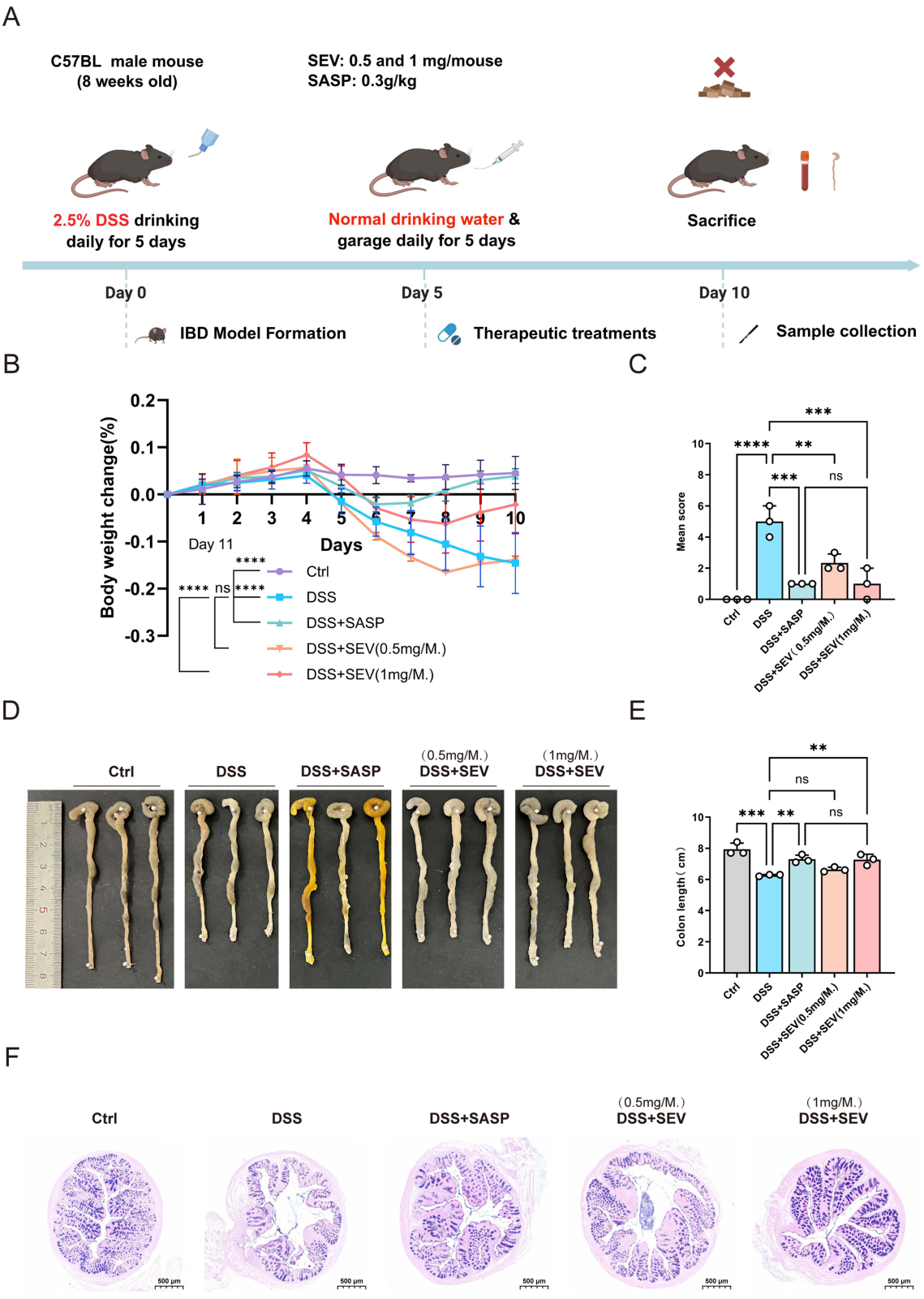

Figure 7 Oral administration of SEV ameliorates disease severity in a DSS-induced IBD mouse model. (**A**) The male C57BL/6 mice were administered 2.5% DSS in drinking water for 5 days to induce colitis, followed by daily oral gavage of SEV (0.5 or 1 mg per mouse) or sulfasalazine (0.3 g/kg) for 5 consecutive days were orally administrated for another consecutive 5 days. Mice were euthanized on day 11 for tissue collection. (**B**) Body weight changes over the experimental period (n = 5). (**C**) Average macroscopic colon scores (n = 3). (**D**) Representative images of colon length. (**E**) Quantification of colon length (n = 3). (**F**) AB-PAS staining showing goblet cell depletion in colonic crypt (magenta: goblet cells, blue: acidic mucins). Scale bar: 500 μm. Data are expressed as mean ± SD. Statistical significance was determined by two-way ANOVA followed by Tukey's post hoc test for (**B**), and one-way ANOVA followed by Tukey's post hoc test for (**C** and **E**); ns $p > 0.05$, $^{**}p < 0.01$, $^{***}p < 0.001$, $^{****}p < 0.0001$.

https://doi.org/10.2147/IJN.S586382

Comprehensive Safety Assessment Confirms the Biocompatibility of SEV as a Therapeutic Platform

To evaluate the biosafety of the SEV for potential therapeutic applications, we first assessed their cytotoxicity in vitro. Cell viability assays demonstrated that SEV exhibited no significant cytotoxicity toward RAW264.7 macrophages and even exhibited a certain pro-proliferative effect ($p < 0.01$ to $p < 0.0001$; Figure 9A). Similarly, SEV also exhibited a favorable safety profile in Caco-2 cells ($p > 0.05$; Figure 9B). To translate these findings in vivo, we administered SEV to healthy mice via oral gavage for five consecutive days. Throughout this period, all animals remained healthy and active, with no significant differences in body-weight between the SEV-treated and PBS control groups ($p > 0.05$; Figure 9C). Further biochemical analysis of serum samples revealed that SEV administration did not cause significant alterations in key hepatic function markers, including alanine aminotransferase (ALT), aspartate aminotransferase (AST), and total protein (TP), or in renal function parameters, including creatinine (CREA) and urea (UREA) ($p > 0.05$; Figure 9D–H). The safety of the SEV was further confirmed by histopathological examination. H&E staining of major organs, including the heart, liver, spleen, lung, kidney, and colon, from SEV-treated mice showed no evidence of tissue damage, inflammatory infiltration, or other pathological alterations compared to controls (Figure 9I). In summary, the safety data presented here support the potential use of orally administered SEV as biocompatible agents. Together with the established anti-inflammatory efficacy, these results warrant further investigation to fully assess the potential of SEV as a natural therapeutic platform for inflammatory bowel disease.

Discussion

PDEV have emerged as natural nanotherapeutics with anti-inflammatory, antioxidant and anticancer properties, owing to their abundant bioactive lipids, proteins and nucleic acids, as well as low their low cytotoxicity and inherent tissue - targeting capacity.[30–32] *S. baicalensis*, a plant rich in bioactive compounds such as baicalin and wogonin, has shown promise in the management of IBD.[33–35] However, the therapeutic potential of SEV in IBD remains unclear. In this study, we establish SEV as a multi-component synergistic therapeutic platform for IBD treatment and investigate the underlying mechanisms.

To facilitate translational application, we developed a simplified two-layer sucrose density gradient isolation method, which streamlines the purification process and improves efficiency and cost-effectiveness compared with conventional four-layer gradients. Characterization of SEV revealed a complex and functionally coordinated molecular composition that collectively supports their role as a multi-component platform. Lipidomic analysis revealed significant enrichment of glycerophospholipids and short-chain fatty acids, which can directly provide energy for intestinal epithelial cells, maintain barrier integrity, and regulate gut microbiota homeostasis.[36] Proteomic profiling indicated that SEV-associated core proteins are involved in energy metabolism, ion homeostasis, antioxidant defense, and biosynthetic processes-functions critically relevant to intestinal epithelial repair and microenvironmental homeostasis. Although miRNAs constitute a minor proportion of sRNAs in the SEV, we identified five known miRNAs (miR166a, miR156, miR164a, miR166b, and miR172) with reported biological activities. Among these, miR166a-3p, found in PDEV from other plant, has been shown to alleviate respiratory diseases and atherosclerosis.[37,38] Most strikingly, metabolomics revealed that SEV carry a range of bioactive metabolites derived from *S. baicalensis*, with flavonoids representing the most abundant class and wogonin as the predominant constituent, which is known for its anti-inflammatory, antioxidant, and antitumor activities.[39,40] Collectively, this multi-component composition – comprising bioactive lipids, regulatory RNAs, functional proteins, and the therapeutic metabolites – positions SEV as a synergistic platform capable of concurrently targeting multiple IBD-associated pathways.

Beyond this compositional synergy, we further demonstrate that SEV exert coordinated functional effects that address two core pathological features of IBD: inflammatory signaling and epithelial barrier disruption. Mechanistically, SEV exert anti-inflammatory effects by suppressing the NF-κB/NLRP3 signaling pathway. In LPS-stimulated RAW264.7 macrophages, SEV treatment downregulated NLRP3 expression and phosphorylation NF-κB p65, resulting in reduced production of pro-inflammatory cytokines, including TNF-α, IL-6, and IL-1β. Simultaneously, SEV increased the expression of the anti-inflammatory cytokine IL-10 and inhibited M1 macrophage polarization. In parallel, SEV directly enhanced intestinal barrier integrity by upregulating Claudin-1 expression in Caco-2 cells. These findings establish that

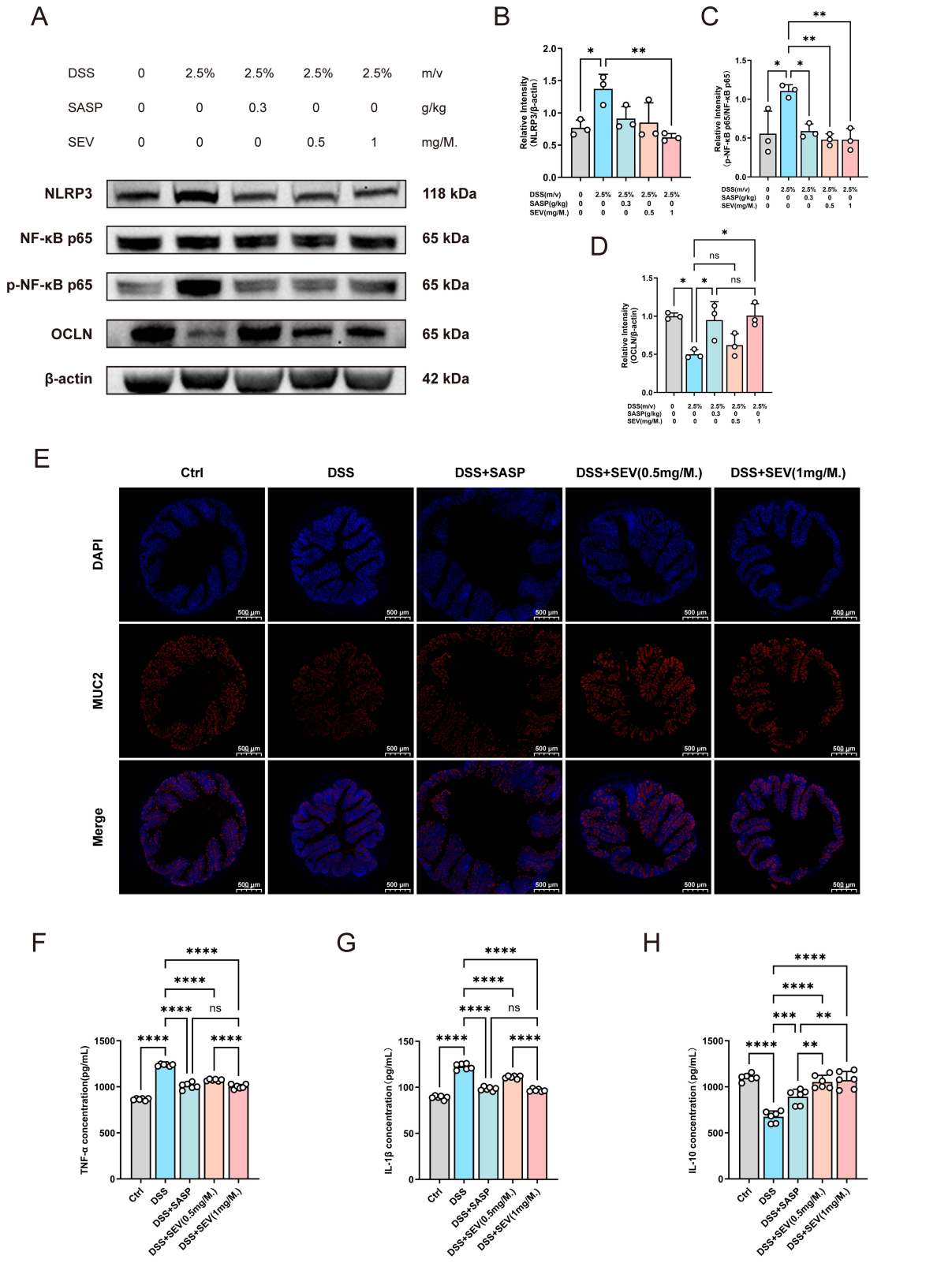

Figure 8 SEV ameliorate DSS-induced colitis through modulation of the NF-κB/NLRP3 signaling pathway and restoration of intestinal barrier integrity. (**A**) Western blot images showing expression of NLRP3, total NF-κB, p-NF-κB, and tight junction protein OCLN in colonic tissues of IBD mice. Representative images from at least 3 independent biological replicates are shown. β-Actin served as a loading control for NLRP3, OCLN; total NF-κB protein was used as a loading control for p-NF-κB. (**B**–**D**) Quantification of protein expression levels. (**B**) NLRP3, (**C**) p-NF-κB, (**D**) OCLN (n = 3). (**E**) Immunofluorescence staining of MUC2 (red) in colonic tissues. Nuclei were counterstained with DAPI (blue). Scale bar: 500 μm. (**F**–**H**) Serum cytokine levels measured by ELISA: (**F**) TNF-α, (**G**) IL-1β, (**H**) IL-10 (n = 6). Data are expressed as mean ± SD. Statistical significance was determined by one-way ANOVA followed by Tukey's post hoc test; ns $p > 0.05$, *$p < 0.05$, **$p < 0.01$, ***$p < 0.001$, ****$p < 0.0001$.

https://doi.org/10.2147/IJN.S586382

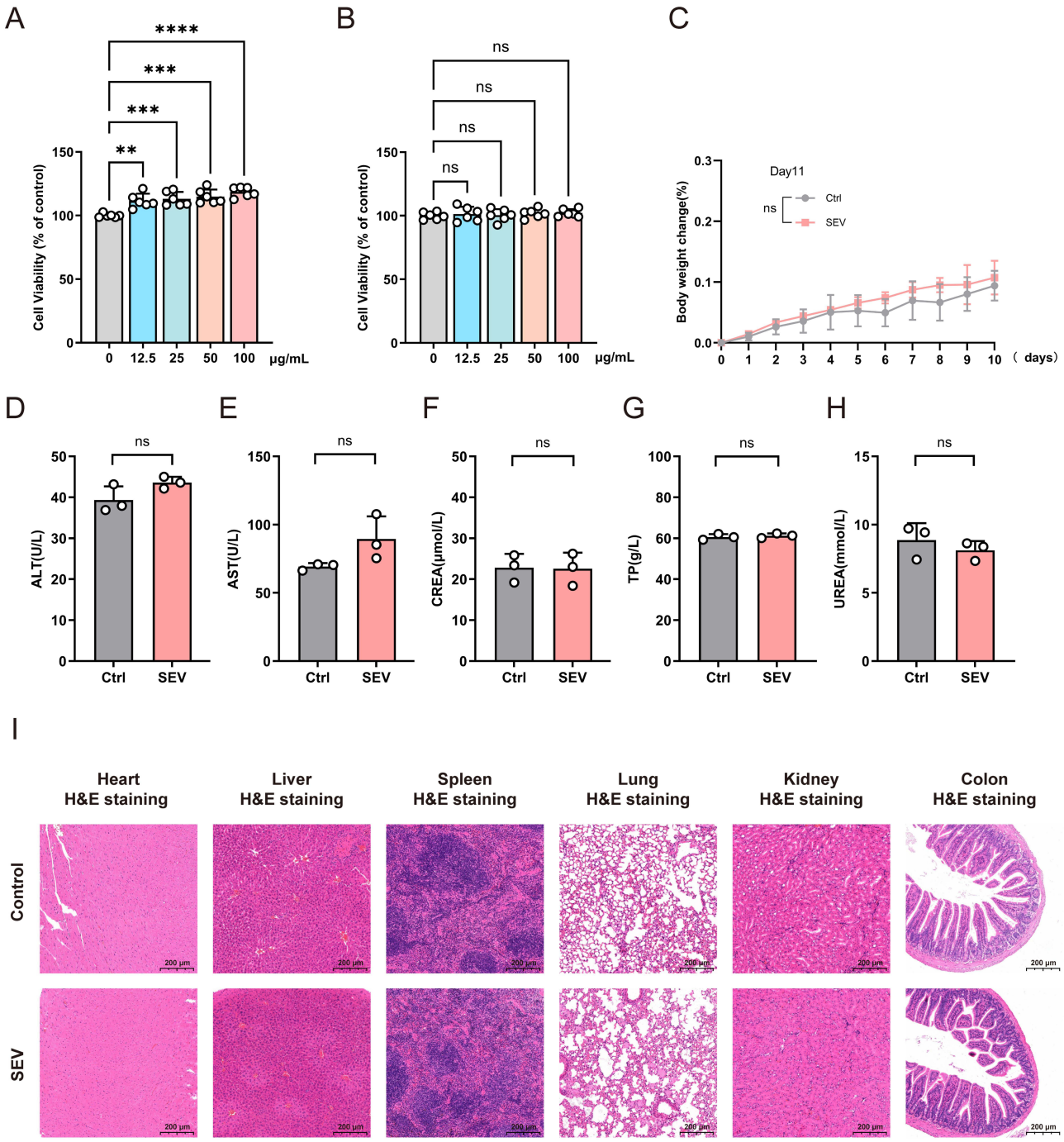

Figure 9 Biosafety assessment of SEV in vitro and in vivo. (**A**) Cytotoxicity evaluation of SEV in RAW264.7 measured by MTT assay (n = 6). (**B**) Cytotoxicity evaluation of SEV in Caco-2 cells measured by MTT assay (n = 6). (**C**) Body weight changes in mice receiving oral administration of SEV (1 mg per mouse) or PBS for 5 consecutive days (n = 5). (**D**–**H**) Serological biochemical analysis of liver and kidney function. (**D**) ALT, (**E**) AST, (**F**) CREA, (**G**) TP, (**H**) UREA (n = 3). (**I**) Histological analysis of major organs. Representative H&E-stained sections of liver, kidney, spleen, heart, lung, and colon from control and SEV-treated mice. Scale bar: 200 μm. Data are expressed as mean ± SD. Statistical significance was determined by one-way ANOVA followed by Tukey's post hoc test for (**A, B** and **D**–**H**); and two-way ANOVA followed by Tukey's post hoc test for (**C**). ns $p > 0.05$, $^{**}p < 0.01$, $^{***}p < 0.001$, $^{****}p < 0.0001$.

SEV integrate anti-inflammatory and barrier-protective functions within a single therapeutic platform, addressing the multifactorial nature of IBD in a coordinated manner.

Consistent with these mechanistic insights, SEV significantly alleviated DSS-induced colitis, as demonstrated by improved macroscopic and histopathological scores and preserved colon length. Building on the established therapeutic

https://doi.org/10.2147/IJN.S586382

dosages of other active components of *S. baicalensis* for IBD,[41,42] this study validated the in vivo efficacy of SEV. Notably, SEV achieved comparable therapeutic effects at a lower dose (1 mg per mouse) than other PDEV (typically 5–20 mg per mouse). Furthermore, compared to synthetic nanocarriers, orally administered SEV demonstrate an inherent ability to target the colon,[43] suggesting that their natural origin may confer favorable biodistribution properties.

When contextualizing our findings within the broader landscape of IBD research, several distinctive advantages of SEV as a synergistic therapeutic platform become apparent. First, their origin from *S. baicalensis*, a traditional herb with a documented use in treating intestinal disorder, may confer inherent intestinal tropism. Second, the enrichment of specific bioactive components, particularly the flavonoid wogonin, within a natural vesicular delivery system represents a novel approach that may enhance stability and confer multi-targeting capacity over conventional small-molecule formulations. Third, the multi-component nature of SEV enables a coordinated therapeutic strategy that simultaneously addresses multiple aspects of IBD pathophysiology, inflammatory signaling, oxidative stress, and epithelial barrier dysfunction, potentially overcoming the limitations associated with single-target approaches. Finally, compared to other medicines, SEV demonstrate a favorable safety profile with no observed cytotoxicity, hepatorenal impairment, or histopathological abnormalities. This finding provides important insights for addressing persistent safety challenges in nanomedicine development.

Despite these promising findings, several questions require further investigation. The relative contributions of specific SEV components to the observed therapeutic effects remain unclear. The precise upstream and downstream mechanisms of NF-κB/NLRP3 pathway modulation also warrant further clarification. The chronic toxicity, immunogenicity, and long-term biodistribution remain to be evaluated. Future studies employing component-specific inhibition, targeted metabolomics, and advanced imaging techniques are essential to fully unravel the complex pharmacology of SEV.

Conclusion

In this study, we successfully isolated nanoscale extracellular vesicles from fresh *S. baicalensis* and established them as novel nanotherapeutic agents for inflammatory bowel disease. We demonstrated that SEV exert dual anti-inflammatory and antioxidant effects on macrophages by specifically suppressing the NF-κB/NLRP3 signaling axis. Furthermore, SEV enhanced intestinal barrier integrity and displayed a favorable safety profile. In a murine model of colitis, SEV significantly alleviated disease severity, suggesting its therapeutic potential. Collectively, this study establishes, for the first time, SEV as a potential novel natural nanovesicle-based therapeutic candidate for IBD, providing an experimental foundation for the translational application of plant-derived vesicles.

Data Sharing Statement

The data supporting our findings are available in the manuscript file or from the corresponding author (Dr. Ruihua Li) upon request.

Ethics Approval and Consent to Participate

No human subjects or clinical samples were included in the study. All animal experiments were performed in accordance with the Institutional Animal Care and Use Committee (IACUC) Guidelines of the Academy of Military Medical Sciences (approval no. SWGCYJS-2025-058). All experimental animals follow the "3R principle". Before the experiment, the animals were adaptively fed for one week, with free access to water and food, maintaining a circadian rhythm, and a temperature of 25 ± 2°C. All animals were humanely euthanized via an intraperitoneal injection of an overdose of pentobarbital sodium (150 mg/kg) to induce deep anesthesia followed by death. Wait after no signs of life. Handle carcass properly and follow ethical guidelines, avoiding sudden and violent methods that could cause intense pain and fear.

Author Contributions

All authors made a significant contribution to the work reported, whether that is in the conception, study design, execution, acquisition of data, analysis and interpretation, or in all these areas; took part in drafting, revising or critically reviewing the article; gave final approval of the version to be published; have agreed on the journal to which the article has been submitted; and agree to be accountable for all aspects of the work.

Funding

This work was partly supported by the Beijing Natural Science Foundation for Young Scholars (grant number: 7244376).

Disclosure

The authors report no conflicts of interest in this work.

References

1. Bruner LP, White AM, Proksell S. Inflammatory bowel disease. *Prim Care*. 2023;50(3):411–427. doi:10.1016/j.pop.2023.03.009
2. Ashton JJ, Beattie RM. Inflammatory bowel disease: recent developments. *Arch Dis Childhood*. 2024;109(5):370–376. doi:10.1136/archdischild-2023-325668
3. Kaplan GG. The global burden of IBD: from 2015 to 2025. *Nat Rev Gastroenterol Hepatol*. 2015;12(12):720–727. doi:10.1038/nrgastro.2015.150
4. Y JJ, E IM, D KIMN. Therapeutic potential of bioactive components from *Scutellaria baicalensis Georgi* in inflammatory bowel disease and colorectal cancer: a review. *Int J Mol Sci*. 2023;24(3):1954.
5. Xia Y, Zhang J, Liu G, Wolfram J. Immunogenicity of extracellular vesicles. *Adv Mater*. 2024;36(33):e2403199. doi:10.1002/adma.202403199
6. Visnovitz T. Extracellular vesicles: biology and therapeutic applications. *Int J Mol Sci*. 2024;25(23):13034. doi:10.3390/ijms252313034
7. Ngo JM, Williams JK, Zhang C, et al. Extracellular vesicles and cellular homeostasis. *Annu Rev Biochem*. 2025;94(1):587–609. doi:10.1146/annurev-biochem-100924-012717
8. Yang S, Li W, Bai X, et al. *Ginseng*-derived nanoparticles alleviate inflammatory bowel disease via the TLR4/MAPK and p62/Nrf2/Keap1 pathways. *J Nanobiotechnol*. 2024;22(1):48. doi:10.1186/s12951-024-02313-x
9. Zhao Q, Feng J, Liu F, et al. *Rhizoma Drynariae*-derived nanovesicles reverse osteoporosis by potentiating osteogenic differentiation of human bone marrow mesenchymal stem cells via targeting ERα signaling. *Acta pharmaceutica Sinica B*. 2024;14(5):2210–2227. doi:10.1016/j.apsb.2024.02.005
10. Wei C, Chen Y, Chen J, et al. miR166u-enriched *Polygonatum sibiricum* exosome-like nanoparticles alleviate colitis by improving intestinal barrier through the TLR4/AKT pathway. *Int J Biol Macromol*. 2025;318(Pt 1):144802. doi:10.1016/j.ijbiomac.2025.144802
11. Yang Y, Yang L, Deng H, et al. *Coptis chinensis*-derived extracellular vesicle-like nanoparticles delivered miRNA-5106 suppresses NETs by restoring zinc homeostasis to alleviate colitis. *J Nanobiotechnol*. 2025;23(1):444. doi:10.1186/s12951-025-03466-z
12. He J, Fu L, Shen Y, et al. *Polygonum multiflorum* extracellular vesicle-like nanovesicle for skin photoaging therapy. *Biomater Res*. 2024;28:0098. doi:10.34133/bmr.0098
13. Hwang JH, Park YS, Kim HS, et al. *Yam*-derived exosome-like nanovesicles stimulate osteoblast formation and prevent osteoporosis in mice. *J Control Release*. 2023;355:184–198. doi:10.1016/j.jconrel.2023.01.071
14. Liu C, Yan X, Zhang Y, et al. Oral administration of *turmeric*-derived exosome-like nanovesicles with anti-inflammatory and pro-resolving bioactions for murine colitis therapy. *J Nanobiotechnol*. 2022;20(1):206. doi:10.1186/s12951-022-01421-w
15. Wang R, Wang D, Wang H, et al. Therapeutic targeting of Nrf2 signaling by maggot extracts ameliorates inflammation-associated intestinal fibrosis in chronic DSS-induced colitis. *Front Immunol*. 2021;12:670159. doi:10.3389/fimmu.2021.670159
16. Talmor-Barkan Y, Bar N, Shaul AA, et al. Metabolomic and microbiome profiling reveals personalized risk factors for coronary artery disease. *Nature Med*. 2022;28(2):295–302. doi:10.1038/s41591-022-01686-6
17. Sho T, Xu J. Role and mechanism of ROS scavengers in alleviating NLRP3-mediated inflammation. *Biotechnol Appl Biochem*. 2019;66(1):4–13. doi:10.1002/bab.1700
18. Chen Y, Ye X, Escames G, et al. The NLRP3 inflammasome: contributions to inflammation-related diseases. *Cell Mol Biol Lett*. 2023;28(1):51. doi:10.1186/s11658-023-00462-9
19. Guo Q, Jin Y, Chen X, et al. NF-κB in biology and targeted therapy: new insights and translational implications. *Signal Transduction Target Ther*. 2024;9(1):53. doi:10.1038/s41392-024-01757-9
20. Naama M, Telpaz S, Awad A, et al. Autophagy controls mucus secretion from intestinal goblet cells by alleviating ER stress. *Cell Host Microbe*. 2023;31(3):433–446.e434. doi:10.1016/j.chom.2023.01.006
21. Yang S, Fan L, Yin L, et al. Ginseng exosomes modulate M1/M2 polarisation by activating autophagy and target IKK/IκB/NF-κB to alleviate inflammatory bowel disease. *J Nanobiotechnol*. 2025;23(1):198. doi:10.1186/s12951-025-03292-3
22. Luo X, Yu Z, Deng C, et al. Baicalein ameliorates TNBS-induced colitis by suppressing TLR4/MyD88 signaling cascade and NLRP3 inflammasome activation in mice. *Sci Rep*. 2017;7(1):16374. doi:10.1038/s41598-017-12562-6
23. Cui L, Wang W, Luo Y, et al. Polysaccharide from *Scutellaria baicalensis Georgi* ameliorates colitis via suppressing NF-κB signaling and NLRP3 inflammasome activation. *Int J Biol Macromol*. 2019;132:393–405. doi:10.1016/j.ijbiomac.2019.03.230
24. Jin X, Liu MY, Zhang DF, et al. Baicalin mitigates cognitive impairment and protects neurons from microglia-mediated neuroinflammation via suppressing NLRP3 inflammasomes and TLR4/NF-κB signaling pathway. *CNS Neurosci Ther*. 2019;25(5):575–590. doi:10.1111/cns.13086
25. D Cui, Qiao W, Chen W, et al. Anti-tumor immunotherapy of *Scutellaria Baicalensis*-derived vesicles on immune checkpoint modulation in colorectal cancer. *Aging Dis*. 2026. doi:10.14336/AD.2026.0040
26. Chen XF, Chen X, Tang X. Short-chain fatty acid, acylation and cardiovascular diseases. *Clinical Science*. 2020;134(6):657–676. doi:10.1042/CS20200128
27. Tian T, Mao Q, Xie J, et al. Multi-omics data reveals the disturbance of glycerophospholipid metabolism caused by disordered gut microbiota in depressed mice. *J Adv Res*. 2022;39:135–145. doi:10.1016/j.jare.2021.10.002
28. Burg T, Van Den Bosch L. Glycerophospholipids in ALS: insights into disease mechanisms and clinical implication. *Mol neurodegen*. 2025;20(1):85. doi:10.1186/s13024-025-00876-3
29. Tao Z, Wang Y. The health benefits of dietary short-chain fatty acids in metabolic diseases. *Crit Rev Food Sci Nutr*. 2025;65(9):1579–1592. doi:10.1080/10408398.2023.2297811

30. Feng T, Wan Y, Dai B, Liu Y. Anticancer activity of bitter melon-derived vesicles extract against breast cancer. *Cells*. 2023;12(6):824. doi:10.3390/cells12060824
31. Kang M, Kang M, Lee J, Yoo J, Lee S, Oh S. *Allium tuberosum*-derived nanovesicles with anti-inflammatory properties prevent DSS-induced colitis and modify the gut microbiome. *Food funct*. 2024;15(14):7641–7657. doi:10.1039/D4FO01366B
32. Tan S, Liu Z, Cong M, et al. *Dandelion*-derived vesicles-laden hydrogel dressings capable of neutralizing Staphylococcus aureus exotoxins for the care of invasive wounds. *J Control Release*. 2024;368:355–371. doi:10.1016/j.jconrel.2024.02.045
33. Yao J, Zhao L, Zhao Q, et al. NF-κB and Nrf2 signaling pathways contribute to wogonin-mediated inhibition of inflammation-associated colorectal carcinogenesis. *Cell Death Dis*. 2014;5(6):e1283. doi:10.1038/cddis.2014.221
34. Zou Y, Dai SX, Chi HG, et al. Baicalin attenuates TNBS-induced colitis in rats by modulating the Th17/Treg paradigm. *Arch Pharmacal Res*. 2015;38(10):1873–1887. doi:10.1007/s12272-014-0486-2
35. Liu C, Li Y, Chen Y, et al. Baicalein restores the balance of Th17/Treg cells via aryl hydrocarbon receptor to attenuate colitis. *Mediators Inflammation*. 2020;2020:5918587. doi:10.1155/2020/5918587
36. Parada Venegas D, De la Fuente MK, Landskron G, et al. Short chain fatty acids (SCFAs)-mediated gut epithelial and immune regulation and its relevance for inflammatory bowel diseases. *Front Immunol*. 2019;10:277. doi:10.3389/fimmu.2019.00277
37. Zhu H, Chang M, Wang Q, Chen J, Liu D, He W. Identifying the potential of miRNAs in houttuynia cordata-derived exosome-like nanoparticles against respiratory RNA viruses. *Int J Nanomed*. 2023;18:5983–6000. doi:10.2147/IJN.S425173
38. Yang R, Lin F, Wang W, Dai G, Ke X, Wu G. Investigating the therapeutic effects and mechanisms of Carthamus tinctorius L.-derived nanovesicles in atherosclerosis treatment. *Cell Commun Signal*. 2024;22(1):178. doi:10.1186/s12964-024-01561-6
39. Ye Q, Huang S, Wang Y, et al. Wogonin improves colitis by activating the AhR pathway to regulate the plasticity of ILC3/ILC1. *Phytomedicine*. 2024;128:155425. doi:10.1016/j.phymed.2024.155425
40. Zhao W, Luo H, Lin Z, et al. Wogonin mitigates Acetaminophen-induced liver injury in mice through inhibition of the PI3K/AKT signaling pathway. *J Ethnopharmacol*. 2024;332:118364. doi:10.1016/j.jep.2024.118364
41. Feng J, Guo C, Zhu Y, et al. Baicalin down regulates the expression of TLR4 and NFkB-p65 in colon tissue in mice with colitis induced by dextran sulfate sodium. *Int J Clin Exp Med*. 2014;7(11):4063–4072.
42. Zhang CL, Zhang S, He WX, et al. Baicalin may alleviate inflammatory infiltration in dextran sodium sulfate-induced chronic ulcerative colitis via inhibiting IL-33 expression. *Life Sci*. 2017;186:125–132. doi:10.1016/j.lfs.2017.08.010
43. Dymek M, Sikora E. Liposomes as biocompatible and smart delivery systems - the current state. *Adv Colloid Interface Sci*. 2022;309:102757. doi:10.1016/j.cis.2022.102757